Eur. Phys. J. A (2016) **52**: 70
DOI 10.1140/epja/i2016-16070-9

THE EUROPEAN PHYSICAL JOURNAL A

Special Article – Tools for Experiment and Theory

Pulse shape analysis and position determination in segmented HPGe detectors: The AGATA detector library

B. Bruyneel[1,2], B. Birkenbach[1,a], and P. Reiter[1]

[1] Institut für Kernphysik, Universität zu Köln, 50937 Köln, Germany
[2] CEA Saclay, Service de Physique Nucleaire, F-91191 Gif-sur-Yvette, France

Received: 18 December 2015 / Revised: 16 February 2016
Published online: 29 March 2016 –
Communicated by A. Gade

Abstract. The AGATA Detector Library (ADL) was developed for the calculation of signals from highly segmented large volume high-purity germanium (HPGe) detectors. ADL basis sets comprise a huge amount of calculated position-dependent detector pulse shapes. A basis set is needed for Pulse Shape Analysis (PSA). By means of PSA the interaction position of a γ-ray inside the active detector volume is determined. Theoretical concepts of the calculations are introduced and cover the relevant aspects of signal formation in HPGe. The approximations and the realization of the computer code with its input parameters are explained in detail. ADL is a versatile and modular computer code; new detectors can be implemented in this library. Measured position resolutions of the AGATA detectors based on ADL are discussed.

1 Introduction

For more than five decades, High-Purity Germanium (HPGe) detectors have been at the heart of powerful spectrometers which allow ever growing insight into the atomic nucleus [1]. Latest developments of HPGe detector technology, instrumentation of data acquisition and processing have led to a refined detection technology which allows to deduce position information from signals of these semiconductor detectors. Especially the digitization of the detector pulses with high resolution, high bandwidth and high sampling frequency over a meaningful time period enables to acquire the pulse shapes of the detector signals. This additional information is exploited to determine the position of charge generation inside the detector volume. In order to localize the scattering sequence following a γ-ray interaction inside a segmented HPGe detector, the experimental pulse shapes are compared to a basis data set of position dependent pulses. For pulse shape analysis (PSA) a huge amount of pulses have to be provided for typically more than 40000 basis sites per crystal assuming a Cartesian grid which is needed to cover the volume of a large HPGe detector.

The reference pulse shapes are collected in lookup libraries. The detailed comparison between reference pulse shapes and measured pulse shapes is in fact the task of PSA algorithms [2–5] which have to identify the most probable interaction position within the active detector material. Meanwhile the two γ-ray tracking spectrometers AGATA [6] and GRETINA [7] are based on PSA of signals from segmented HPGe detectors to obtain position information on the interaction of γ-rays.

There exist two different procedures to generate the basis set of pulse shapes: it can be obtained from experiment with the existing detectors or the pulses are the result of a calculation which takes all the relevant aspects for a final comparison with measured information into account. For the experimental solution dedicated scanning tables have been developed for the large HPGe detectors in recent years. The scanning table uses a heavily collimated γ-ray source, usually a very strong ^{137}Cs source producing a pencil beam of gamma-rays to select interactions taking place at a particular position inside the detector volume. The x, y-coordinate of the collimator position defines one part of the coordinates of the interactions, whereas the coincident detection of a Compton scattered γ-ray inside a secondary collimation system completes the event selection. The interaction position in the z-direction inside the germanium is then defined by the intersection of both collimator openings. Multiple interactions are suppressed by requiring additional conditions on the detected energy. Such scanning systems have been built in Liverpool [8, 9], Orsay [10], Salamanca and Strasbourg [6]. At GSI, Darmstadt a technique based on positron annihilation was suggested [11, 12]. However, such scanning methods are very time consuming, such that until now, the required reference pulse shape libraries could not be entirely established by measurement alone. Development

[a] e-mail: birkenbach@ikp.uni-koeln.de

of faster characterization procedures [13,14] are therefore still of high interest. After such characterization, the error between simulation and experiment can be brought down to less than 2% of the full energy signal [15]. However, the extremely time consuming nature of the experimental scanning methodology favours the more practical way to generate a full basis of pulses by calculation.

The AGATA spectrometer employs PSA to determine the positions of the interaction points with a much higher position resolution than the physical segmentation of the detector volume [16]. A γ-ray causes typically a chain of interactions in the germanium detectors (*e.g.* 3–4 interaction points at an energy of 1.3 MeV). There can be more than one interaction in one segment of a detector and the γ-ray can be scattered to another segment of the same crystal or to an adjacent detector. A high precision of the interaction positions is required in order to perform the subsequent γ-ray tracking with high accuracy [17,18]. For the design of AGATA a position resolution of 5 mm (FWHM) was assumed [19]. The preamplifier signals of all 36 segments and the core electrode of every detector are digitized using a 14 bit analogue to digital converter with a rate of 100 MHz. The large dataset from the single crystal are compared to the calculated existing set of signal pulses. This comparison includes the signal of the core electrode, the signal of the hit segment electrode and the signals from the neighboring segment electrodes for every interaction. This is needed because the size and shape of the bipolar transient signals induced in the neighboring segment electrodes contain the important information for the angular and z position of the interaction. In the case of AGATA, a detector crystal has a large volume of $\cong 380\,\mathrm{cm}^3$ and a weight of $\cong 2\,\mathrm{kg}$. The required PSA libraries typically contain over 10^5 reference pulse shapes. Combined with the segmentation of the capsule, the PSA achieves position resolutions of about 4 mm FWHM [20] for the AGATA detectors.

In order to generate a data base for looking up the individual positions inside the Ge detector volume the pulses are calculated by performing an elaborate detector characterization which includes a minimum of input parameters to simulate the complete detector response after the γ-ray interaction. For this reason simulation codes for HPGe detector have been developed within the AGATA Collaboration: the Matlab based Multi Geometry Simulation code (MGS) [21,22], the Java AGATA Signal Simulation toolkit (JASS) [23] and the AGATA Detector Library (ADL) which is subject of this publication. ADL data basis were employed for PSA of all in-beam experiments with the AGATA detectors up to now.

In the first part of the paper the general concepts and basic assumptions are introduced. The following sections explain the calculations of electrical fields, charge carrier mobilities and mirror charges. The experimental impact of the response function and the crosstalk contributions are explained next. Main part of the paper is the section on the ADL code describing its structure, the detailed calculations of the various subroutines and the determination of accurate input parameters for individual Ge crystals. At the end the achieved results on position resolution are presented and discussed.

2 Simulating HPGe detectors

Semiconductors in general are described by the Van Roosbroek equations [24] which, aside from the Poisson equation for the electrical field, also comprises continuity equations for the electron and hole densities. For the silicon industry, commercial packages like Silvaco [25] and Synopsys [26] are available to solve these equations. However, even for experts, solutions to the Van Roosbroeck equations are generally not trivial to obtain. Convergence of the solution is often critically related to a proper choice of grid, which already implies a fair knowledge in advance on the expected solution. Luckily, for the simulation of large volume germanium detectors for gamma-ray detection, several approximations can be applied, which simplify the problem drastically.

2.1 Delta interactions

Radiation interacts with the active detector material by creating electron hole pairs. Depending on the type and the energy of the radiation the volume of the created charge cloud changes. For example a single interaction of a 1 MeV γ-ray in germanium knocks out fast electrons that loose their energy by creating electron-hole pairs resulting in a charge cloud with a radius of 0.5 mm [23]. For γ-ray energies above 250 keV, independent of the initial gamma-ray energy, the initial energy will be statistically broken up in energy deposits of 100 to 250 keV due to Compton scattering [17]. This energy interval is defined by the region where the Compton cross section is taking over from the photo absorption. The range of a 100 keV photo-electron in germanium is only 44 μm [27]. Even in the statistically unlikely event of a 1 MeV photo absorption, the range of the 1 MeV photo electron is still only 1.2 mm, which is still less but comparable to the achievable position resolution. Thus all interactions by γ radiation can typically be considered as point like interactions, as the range of the electrons cannot be resolved.

2.2 Plasma erosion time

However, a partial shielding from the external field occurs in the detector immediately after the creation of electron hole pairs, that causes a tiny time delay required to separate the electrons and holes. This shielding effect significantly affects the PSA for particle identification in silicon detectors [28]. It roughly scales with the stopping power along the particle track and is inverse proportional to the external applied field. In silicon particle detectors, the ionization density along particle tracks is so high that partial shielding from the external field occurs. As a consequence an increase in the rise time is observed due to the additional time required to separate electrons and holes from

the initial plasma. Typical values for the plasma erosion time τ_{pl} are 1–3 ns for alpha particles and 2–5 ns for heavy ions [29]. The plasma erosion time scales proportional to the square root of the stopping power along the particle track, and inverse proportional to the external applied field E_0 [28]:

$$\tau_{pl} \propto \frac{1}{E_0} \cdot \sqrt{\frac{\mathrm{d}E}{\mathrm{d}x}} \,. \tag{1}$$

Although the quoted time constants are already small compared to the typical collection times of several 100 ns in large volume HPGe detectors, the effect will be even more reduced considering the stopping power of photoelectrons in germanium is about two orders of magnitude smaller than for alpha particles at 100 keV. From this we conclude it should be safe to neglect plasma erosion times.

2.3 Diffusion

Under action of diffusion, initial delta distributions will be transformed into a Gaussian distribution of size

$$\sigma = \sqrt{2Dt}. \tag{2}$$

The diffusion coefficient for electrons and holes at LN2 temperatures in germanium [30] is less than $D < 300\,\mathrm{cm}^2/\mathrm{s}$. Typically collection times in an AGATA detector will not surpass $0.6\,\mu$s. This gives an upper limit of $\sigma_{\max} < 0.2\,$mm. The image charges induced in each electrode by such Gaussian profiles will not differ substantially from the image charges induced from a delta distribution. Diffusion effects are therefore neglected in ADL. Exceptions exist when the charge collection is happening in the vicinity of a segmentation border. The gap between segments has been measured to vary between 0.09 mm and 0.72 mm on AGATA detectors [31]. Diffusion should be included to properly describe the charge sharing between both electrodes in these cases.

2.4 Quasi-static field approximation

In all our calculations, the finite speed of light is neglected, such that image charges at electrodes in the detector are created instantaneously in response to charges created in the bulk of the detector. At any point in time the detector is therefore considered to be in an electrostatic equilibrium. A sufficient condition for this to be true is that the time required for light to cross the detector volume is negligible compared to the timing accuracy required in the calculation. The quasi-static approximation is readily assumed in the Van Roosbroeck equations, and is, further, also a prerequisite for the Ramo theorem (discussed further in the text) to be valid. Furthermore, it is assumed that the extra field generated by the charges created by the gamma radiation is negligible compared to the external applied collection field.

In summary, electrons and holes created by γ radiation in large volume germanium detectors are approximated as traveling independently in a fixed applied field, and without appreciable diffusion, which represents a serious reduction in complication.

3 Ingredients of signal calculation

According to the introduced approximations the requirements for numerical signal calculation are separable: i) Calculation of the fixed electric field in the reverse biased detector. ii) The mobility of electrons and holes are needed to calculate their respective trajectories under action of the external field. iii) Calculation of the instantaneously induced image charge in any electrode of the detector as a function of the positions of free electrons and holes in the depleted region of the detector. iv) The different inputs (potentials, mobility, mirror charges, response functions) have to be generated and combined for the final calculation of the electric signals in the detector. The various parts are introduced and explained in the following subsections.

3.1 Electrical field

First the electrical field inside the detector has to be calculated. Depending on the geometry of the detector, this is done analytically or numerically. An analytical example is the true coaxial detector[1] which resembles the AGATA detector to a major fraction. The Possion equation,

$$\Delta\phi = -\frac{\rho}{\epsilon}\,, \tag{3}$$

in cylindrical coordinates becomes

$$\frac{\mathrm{d}^2\phi}{\mathrm{d}r^2} + \frac{1}{r}\frac{\mathrm{d}\phi}{\mathrm{d}r} = -\frac{\rho}{\epsilon}\,.$$

The core electrode of a true coaxial detector defines the inner radius r_1 and the outer electrode the outer radius r_2. The boundary condition is the applied voltage V between the two electrodes $\phi(r_2) - \phi(r_1) = V$. Solving the equation for $E(r) = -\frac{\mathrm{d}\phi}{\mathrm{d}r}$ results in

$$-E(r) = -\frac{\rho}{2\epsilon} + \frac{V + \left(\frac{\rho}{4\epsilon}\right)\left(r_2^2 - r_1^2\right)}{r \ln \frac{r_2}{r_1}}\,,$$

assuming the space charge as constant.

The solution to the Poisson equation for a more complex geometry is obtained numerically by a finite differencing technique on a cubic grid. The cubic grid was chosen as it fits well with most geometries and has some non-negligible advantages compared to irregular meshes. It simplifies drastically the equations after discretization, which in addition results in more numerical stable solvers. The structured grid allows for a fast lookup and interpolation of the values compared to irregular meshes.

[1] See, for example, [29] page 422.

Homogeneous Neumann boundary conditions are applied to the array boundaries. The potentials have no gradient component tangential to the array boundaries. The homogeneous boundary condition is typically also used for the passivated layer on the backside of the AGATA crystals. However, this is a convenient approximation. The correct boundary equation for passivated areas is given by:

$$n \cdot \epsilon_0(\epsilon_1 E_1 - \epsilon_2 E_2) = \rho_s, \tag{4}$$

with n, a local unit vector normal to the surface. E_1, $\epsilon_0\epsilon_1$ is the field and the permittivity near the boundary on the inside of the detector. E_2, $\epsilon_0\epsilon_2$ are similar quantities just outside the detector. The boundary condition thus relates the field component normal to the detector boundary surface to the field outside the detector, and an influence due to the encapsulation exists. Moreover, passivation layers possess a surface charge density ρ_s. This surface charge density on the passivation layer is difficult to be controlled during manufacturing, and is very temperature dependent [32]. Details of the passivation layer (geometrical size, thickness and charge density) are not available from the manufacturer[2] after encapsulation of the HPGe crystal.

For these reasons, the passivated surface is approximated by a homogeneous Neumann condition:

$$n \cdot E_1 = 0. \tag{5}$$

Under this approximation, small deviations between simulation and experiment are expected for example in the rise time profiles. This was observed as a result of an ^{241}Am source scan where the cylindrical surface at about 1 cm from the back of the passivated layer was irradiated with very low energy γ-rays (for details see [15]). The mobility at the passivated surface boundaries is known to be much below the bulk mobility [33], also enhanced trapping and diffusion is expected to play a significant role for the signal formation. Fortunately this behavior is limited to the very back of the long Ge crystal and only a minor fraction of the deposited γ-ray energies are affected by these effects.

3.2 Charge carrier mobility models

In contrast to planar detectors, the anisotropic behavior of the moving charge carriers is of high importance in large coaxial detectors. The field orientation can take any direction with respect to the crystal orientation. Differences in mobility between fields along different crystallographic axes differ up to about 30% in the high field regime. A correct description of the mobility is therefore key to a precision simulation of HPGe detectors.

Rise time measurements [34] are performed to characterize the crystal orientation of the detector. The orientation of the asymmetric AGATA crystals were measured [34]. The method is based on the use of a collimated 400 kBq ^{241}Am source emitting 60 keV γ-rays in combination with a small lead collimator of 1.5 mm radius and

[2] CANBERRA Industries Inc.

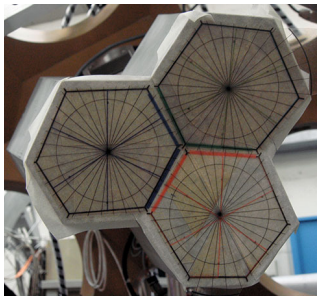

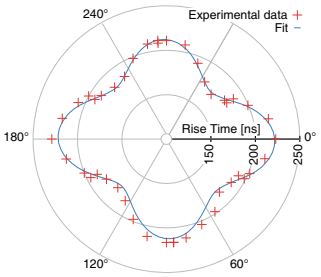

Fig. 1. Aligned masks for scanning the crystal axis (left) and rise times depending on the angular position of the collimator for the asymmetric AGATA detector B002 (right).

1 cm length. The low energy γ-rays deposit their energy within a few millimetres of the active detector material. The created holes are collected immediately and only the drifting electrons form the signal.

The crystal is scanned from the front over a circle with a fixed radius of 2.35 cm. The differences in rise time between different angles result mainly from the crystal internal structure. The impact of the hexagonal shape of the crystals is reduced. A mask, see left picture in fig. 1, indicating 32 different scanning angles was placed at the front face of the detector. The mask was aligned by requesting that the count rates of two neighbouring segments are equal when the collimated source is placed on the corresponding segmentation line and that at the centre of the mask all front segments showed nearly equal count rates. The data acquisition recorded the energy and the full trace signals of every event. In the analysis the signals were filtered for total energy deposition and an average trace was build for every scan position. An example for the resulting 10% to 90% rise time is shown in the right plot of fig. 1 for the AGATA detector B002. The applied fit function is

$$T_{10}^{90}(\theta) = A \cdot (1 + R_4 \cdot \cos(4 \cdot (\theta - \theta_4))) \cdot (1 + R_2 \cdot \cos(2 \cdot (\theta - \theta_2))),$$

with A, R_4, R_2, θ_4 and θ_2 as fit parameters. The largest contribution comes from the second factor that models the 4 fold symmetry of the anisotropic mobility. θ_4 describes the crystal orientation. The R_2 term corrects for small observed deviations of the 4 fold symmetry caused by the asymmetric shape of the detector. The results show clearly the orientation of the axis. We observed this orientation to be the same for all detectors.

Both electrons and holes move fastest in the direction of the crystallographic $\langle 100 \rangle$ axis (near 45° - see right plot of fig. 1). Moreover, this asymmetry in the drift velocity causes components in the drift velocity tangential to the applied field. The orientation of these tangential components is always oriented towards the nearest $\langle 100 \rangle$ axis. However, for symmetry reasons, when the field is applied in the direction of a crystallographic symmetry axis, these components vanish. For the required mobility as function of field strength, full three dimensional mobility models were developed both for electrons [35] and

holes [36]. These models are specific to mobility in germanium near liquid nitrogen temperature (77 K).

3.3 Mirror charges

Once the trajectories of all free charges in the detector are calculated in function of the time, the induced signals in each of the electrodes can be determined. Hereto one calculates the weighting potential for each of the electrodes of interest, for every position in the sensitive volume of the detector. By definition, this weighting potential $\phi_i(\boldsymbol{x})$ equals the induced charge Q_{ind} in electrode i for a unit of charge placed at position x in the detector. For a charge q at this position, we therefore get, by definition,

$$Q_{\mathrm{ind},i} = -q\phi_i(\boldsymbol{x}). \tag{6}$$

The Ramo theorem [37] provides a very attractive solution to the problem of calculating these weighting potentials. It assumes that all electrodes are kept at fixed potential, such that in a small AC signal perturbation approach, these electrodes can be considered grounded. Under these circumstances, the weighting potentials are obtained as solution to the Laplace equation:

$$\nabla^2\phi_i(\boldsymbol{x}) = 0 \qquad \phi_i|S_j = \delta_{i,j}. \tag{7}$$

The boundary conditions to this problem can be readily extracted from the definition: If a charge is closely positioned to the electrode with surface S_i, the total of induced charge in that electrode will be $Q_{\mathrm{ind}} = -q$, or the weighting potential at electrode i should take the homogeneous Dirichelet condition $\Phi_i|S_i = 1$. If, on the contrary, the charge q is placed close to another electrode $j \neq i$, then the total image charge will be induced in electrode j. This has as consequence that all other electrodes will see no net charge in the detector as the charge q is totally screened by the image charge. Therefore the boundary condition for any other electrode $j \neq i$ should take the homogeneous dirichelet condition $\Phi_i|S_j = 0$. This explains the use of the delta function in eq. (7).

In this picture the time evolution of the induced charge, and thus the integral of the current flown into this electrode is given simply by the charge weighted sum of the weighting potential evaluated at the momentary position of the free charges:

$$Q_{\mathrm{ind},i}(t) = -\Sigma_q q\phi_i(\boldsymbol{x}_q(t)). \tag{8}$$

By differentiation of eq. (8) it can be proven that the induced current by the movement of charge q is given by

$$I_{\mathrm{ind},i} = -q\boldsymbol{v}_d \cdot \nabla\phi_i(\boldsymbol{x}), \tag{9}$$

with $\boldsymbol{v}_d$ the momentary drift velocity of the charge q. The inverted gradient of the weighting potential is called weighting field. Within ADL, eq. (8) is preferred over eq. (9) in the calculation of the induced signals, as usually charge sensitive preamplifiers are used. Moreover, even in case current sensitive preamplifiers are used, this method is preferred, since the evaluation of the gradient in eq. (9) is introducing unnecessary calculation errors in the simulation.

It has been proven [38] that the weighting potentials are not affected by the possible presence of space charge in the medium. Hence the right-hand side of eq. (7) is zero. This can also be simply argued: the image charges generated to deplete the space charge were generated while biasing the detector, and therefore do not need consideration in the small signal AC equivalent scheme which describes the perturbation of the steady state of the detector.

It was silently assumed that the detector medium was uniform. In case different materials are used, the Ramo theorem will need modification. If furthermore resistive materials are used (for instance the detector is not fully depleted), then the modified equation to solve is [39]

$$\nabla(\epsilon(\boldsymbol{x}) + \sigma(\boldsymbol{x})/s)\nabla\phi_i(\boldsymbol{x}, s) = 0, \tag{10}$$

where the ϵ and σ represent the position-dependent permittivity and conductivity of the detector medium. The parameter s is a complex frequency as used in the Laplace transform. Upon inverse Laplace transformation, the weighting potential becomes now time dependent.

3.4 Electronic response and crosstalk

The charge signal as calculated using the Ramo theorem, will need convolution with a realistic response function of the acquisition electronics. The response function of the preamp can usually be measured by injection of a clean fast rectangular pulse in the preamplifiers pulser input. By using eq. (8) rather than eq. (9), we took already the time integration into account, such that we only have to convolute with the time derivative of the measured preamplifier response to obtain realistic signals.

However, since all channels in a highly segmented detector are not grounded, but connected to a preamplifier, the ideal Ramo currents, as described by eq. (9), will not strictly apply and needs modification. This effect is on the origin of fundamental cross talk in segmented detectors and can be described by an extension to the Ramo theory [38]. This model was worked out in the particular case of AGATA detectors [40], and found in good agreement with experimental results.

For AGATA detectors, the crosstalk has been observed to contribute two types: the proportional crosstalk, which creates a crosstalk signal in neighboring electrodes proportional to the capacities between the electrodes involved. This type of crosstalk can be described by assuming the preamplifier acts at low frequencies as a large (Miller equivalent) capacitance on the collecting electrode. Accurate routines were developed to measure and correct for this type of crosstalk within AGATA [41].

Proportional crosstalk in AGATA detectors creates additional contributions to the charge carrier signals in neighboring electrodes which is proportional to the time derivative of the driving signal. This type of crosstalk can be described by the fact that at higher frequencies, the

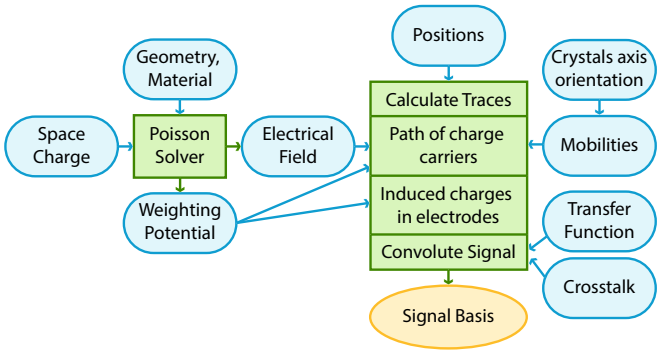

Fig. 2. Block diagram of the routines (green) and the input (blue) for an ADL simulation.

input of the preamplifier starts acting as a resistor. Measurement of derivative crosstalk in practice is oft very difficult as it is usually superposed on real transient signals. Nevertheless, also this type of crosstalk is growing proportional to the capacities between the electrodes involved, and shows correlation with the proportional crosstalk [42].

4 AGATA Detector Library

The AGATA Detector Library is written in the computer language C. It is used for realistic simulations of semiconductor detectors in nuclear physics in general. In the following discussions the focus concentrates on highly segmented HPGe coaxial detectors, although many points can be transferred to different geometries or semiconductor materials.

4.1 Layout of the ADL software

In fig. 2 a block diagram of the ADL is shown. The routines are colored in green and the user provided input is colored blue. The main routine called `Calculate Traces` consists of three subroutines and takes the interaction position as input. The first subroutine calculates the path of the charge carriers through the detector material for every time step. It needs the electrical field and a mobility model of the charge carriers as an input. The second subroutine calculates for every time step the induced charges in all electrodes. It needs the weighting potentials to do this. The last subroutine convolutes the signal with predefined functions. The routines and their input parameters will be described in detail within the next sections.

ADL intents to be flexible and extendable. The library has a special registration of the routines and input parameters controlled by template files. An overview of the parts of ADL is given in table 1.

4.2 Calculating the weighting potentials and the electrical field

First the electrical field and the weighting potentials [43] have to be calculated. The ADL library provides basic geometries like the true coaxial or a planar detector. More complex geometries are provided as SIMION [44] potential arrays. The user can easily add new geometries as SIMION potential arrays or implement new routines to add different formats.

Table 1. Components of the ADL software which is controlled by template files.

Parts	Description
ADL	Main setup file
CONVOLUTION	Convolution of transfer function
DRIFT	Charge carrier mobility models
EVENT	Basic event information
FIELDS	Geometries, weighting and electrical fields
READWRITE	Input and output
TIME	Timing filter settings
TRACES	Calculation of traces
TRAPPING	Trapping sensitivities and path length

The weighting potentials are determined by a 3D Poisson solver which is implemented in the library to calculate the fields. It is based on the established technique of successive over relaxation [45]. For this reason the detector is split into many small cubes called voxels. Each voxel is either an electrode or active detector material. To calculate the weighing potential for one electrode, this electrode is set to 1 V and all other electrodes are set to 0 V. The solver now iterates over all voxels. If the voxel is active material, it takes the average of the values of the 6 neighbouring voxels as its new value plus some over relaxation parameter for faster convergence. If the voxel is an electrode, it is not changed. The value change is monitored and if it becomes small enough the calculation stops. The field solutions are stored in a format compatible with the commercial code SIMION.

In order to check the reliability of the numerical results, the numerical solution of the solver was compared to the analytic one. The comparison shows only small deviations in the per mille range at the boundaries.

Different parameters can be adjusted in the template files depending on the type of input. For the analytical solvable geometries the applied high voltage, the impurity concentration, geometric details and the relative permittivity of the medium are set. For the SIMION files the different weighting potentials for all electrodes and the contribution of the impurity concentration must be given as file input.

For all AGATA geometries SIMION files were calculated and are available from the IKP AGATA webpage [46]. To create a full simulation of an AGATA detector the weighting potential for all 36 segment and the core electrode have to be calculated. An example of a weighting potential of detector A001 as calculated by the ADL routines is shown in fig. 3. On the top panel, a slice through

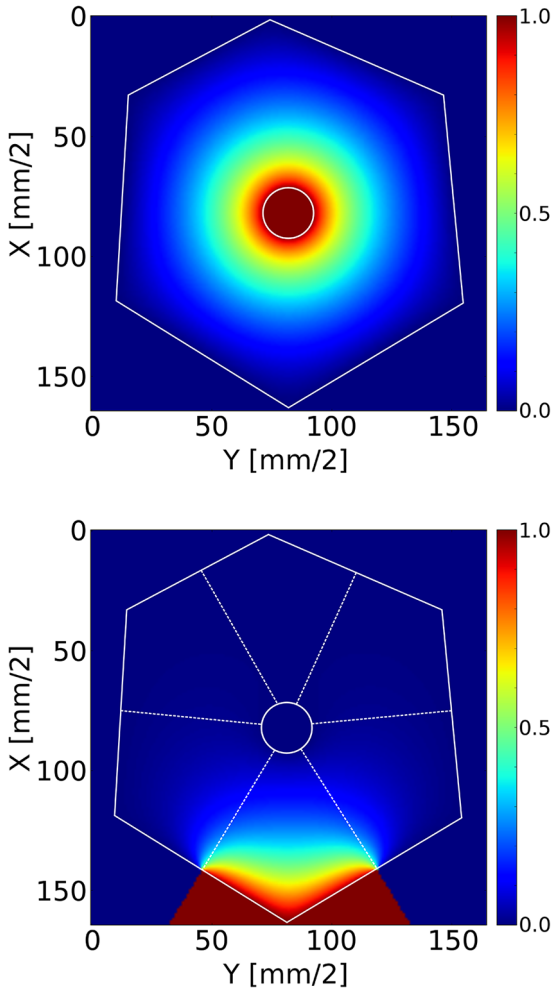

Fig. 3. Weighting potentials for the core electrode (top) and segment electrode A4 (bottom) of detector A001. The slices are taken at 40.5 mm from the front of the detector. The complete region outside the active germanium material are marked as electrodes with a fix potential of 1 V. The units of the z-scale are Volt.

the weighting potential of the sixfold segmented detector in the coaxial part of the detector is depicted. On the bottom plot, the weighing potential of segment A4 is presented. From the weighting potential values on the boundary between the nearest neighbour and second nearest neighbour of A4 it can be seen that the amplitude of transient signals will be limited to 2–3% of the hit segment signal for second nearest neighbours. The plot demonstrates that nearest neighbouring segments contribute predominantly to a detectable amplitude in transient signals.

The electrical field is the weighting potential of the core electrode scaled by the applied bias voltage plus the field created by the space charge distribution. The space charge is the uncompensated net impurity charge density of the germanium material. The contribution of the space charge to the electrical field is the calculated electrical field of the distribution for the boundary electrodes set to 0 V.

Table 2. Parameters for the mobility of electrons and holes in germanium according to the parametrization given in [15] (see eq. (7)). The inter valley scattering rate for the electron mobility is the second-order expansion of eq. (8) in [36].

Electron mobility parameters			
Mobility along ⟨100⟩		Inter valley scattering rate	
E_0 [V/cm]	507.7	E_0 [V/cm]	1200
β	0.804	ν_0	0.459
μ_0 [cm^2/V s]	37165	ν_1	0.0294
μ_n [cm^2/V s]	−145	ν_2	0.000054
Hole mobility parameters			
Mobility along ⟨100⟩		Mobility along ⟨111⟩	
E_0 [V/cm]	181.9	E_0 [V/cm]	143.9
β	0.735	β	0.749
μ [cm^2/V s]	62934	μ [cm^2/V s]	62383

For the simulations of the AGATA detectors the impurity profiles provided by the manufacturer are used. As it is possible to measure the impurity concentration of encapsulated germanium crystals [47–49], the information of the manufacturer were verified by independent pulser measurements for the first asymmetric AGATA detector systems [50].

4.3 Calculation of pulse shapes

Radiation interacts within the active detector material by creating electron-hole pairs. For the simulation the interaction positions and the deposited energies are given as an input. A simple event structure is implemented that allows to set the maximum number of simultaneous interactions per event, the number of electrodes, the number of time steps and the time resolution (step size). Once the charges are created inside the active Ge material, they travel along the electric field of the reversed biased semiconductor detector and induce a signal in the electrodes. The quasi-static field approximation is applied, such that the induced signals at all electrodes of the detector are instantaneously created. The time to collect all charge carriers is depending on the geometry of the detector, the applied voltage and the impurity concentration of the semiconductor material. The two charge carriers have different mobilities resulting in different collection times for electrons and holes. Different models are provided by the library for the mobility. A basic model assumes a constant mobility. Another implemented model, see [29] p. 434, assumes an empirical dependence of the drift velocities with the electrical field strength. However electron and hole mobilities in germanium are not isotropic, but depend on the orientation of the crystallographic axis of the cubic centred germanium crystal structure with respect to the electrical field. Recent publications [15, 35, 36] show, that such anisotropic treatment of electron and hole mobilities is crucial in non-planar coaxial detectors. A realistic model of the mobility inside germanium crystals is implemented. The parameters described in [15, 36] are listed in table 2.

The routines that calculate the path of the charge carriers along the electrical field are based on the 5th-order Runge Kutta integration method with adaptive step size control (from [45] chapt. 16.2, p. 714). The induced signals for every electrode of the detector are calculated depending on the drift of the electrons and holes to the electrodes. For every time step and for each interaction the weighting field evaluated at the position of the electrons is subtracted from the weighting field evaluated at the position of the holes. These differences are multiplied by the charge produced at the individual interaction. The sum of all interactions results in the signal set for the given event.

Finally these traces are convoluted with realistic behaviour of the detector system. The different polarity of the preamplifiers are set up as a convolution function. The transfer function of the preamplifier or the cross talk of segmented crystals could be taken into account. Actually in the online analysis of AGATA these functions are folded in the signals of the library, as they could vary for different detector and digitizer configurations.

Additionally the library provides routines to calculate the trapping sensitivities relevant for neutron damage correction as described in [51]. The trapping sensitivities are added to the PSA bases and are used in the neutron damage correction of the AGATA online analysis.

4.4 Building AGATA PSA bases

In the following example a simulation for the detector A001 is described in more detail. The computer program that calculates a PSA base for AGATA iterates over the active detector volume with a defined grid size. In AGATA a 3D grid size of 2 mm is used. For an A type detector 47156 positions inside the detector volume are calculated. The applied high voltage for the detector is 5000 V. To calculate the charge collection process the anisotropic mobility model is used including the measured axis orientation. Single interactions are calculated with an energy deposition of 1 keV. The trace length is set to 600 ns with a 5 ns step width. In addition to the trace signals the trapping sensitivities for the online neutron damage correction are calculated for every position.

In fig. 4 the resulting simulated traces for AGATA detector A001 are summarized. On the top plot, the core signal for different interaction radii are shown. The effect of the different mobilities of electrons and holes is clearly visible. For small radii the faster electrons are collected immediately while the slower holes still have to drift to the segment electrode. The shortest rise time occurs at an intermediate position, where the collection process for both signals is equal. Then for larger radii the time of the electrons to be collected is longer than for the holes, as they have to drift to the core electrode. On the bottom plot of fig. 4 the transient signals in a segment next to the hit segment are shown. Depending on the distance of the interaction to the non hit electrode, the amplitude of the transient signal changes.

The calculated PSA base sets are used in the AGATA online and offline analysis. In fig. 5 the best match of a

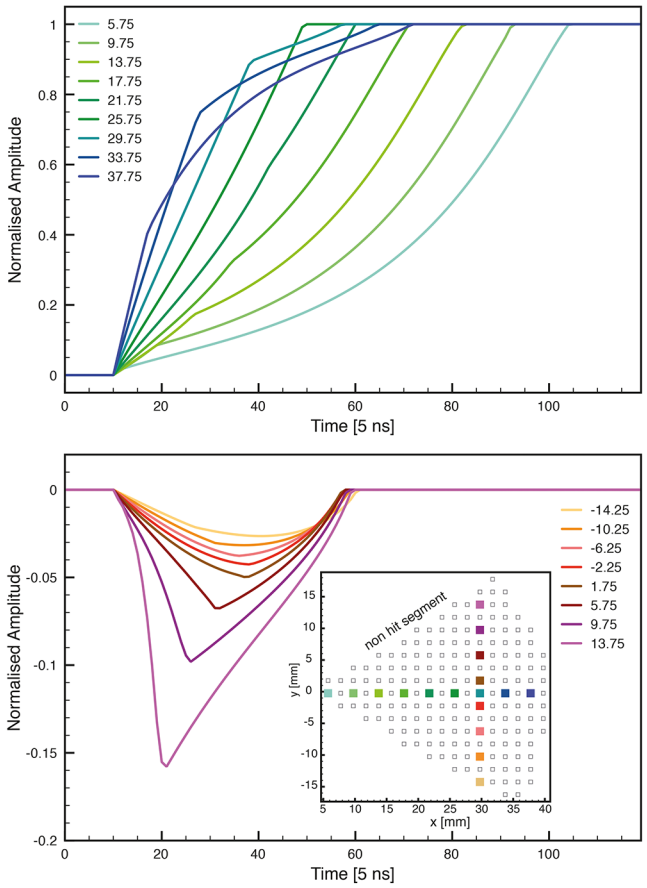

Fig. 4. Simulated traces for an AGATA detector. Top shows the core signal for different radii and bottom shows the transient signals induced in a non hit neighbouring segment. Colour code as indicated in the inset of the bottom graph. The slice is at 40.25 mm from the front of the detector.

random interaction scaled to the right energy is compared to the experimental data. The plot shows a so called super trace. The individual trace of all segment electrodes and the core electrode with a length of 600 ns are plotted after each other. The different electrode sections are marked by the axis label. In the bottom plot the absolute difference between the traces is shown.

All calculated PSA bases for the AGATA detectors are available through the following AGATA web page [46].

4.5 Position resolution obtained with ADL bases

For AGATA the PSA runs as part of the data acquisition process already online. For this purpose a set of fast PSA algorithms, such as grid search [2], genetic algorithms [3], wavelet decomposition [52], a matrix method [4] and a particle swarm algorithm [5], were developed. All algorithms compare the recorded pulses with a database that holds signal pulses of defined positions in the detector. The signal library includes all signal traces over a 2 mm grid. Before the search algorithm is applied the distortion by the electronics is taken care of by folding the transfer

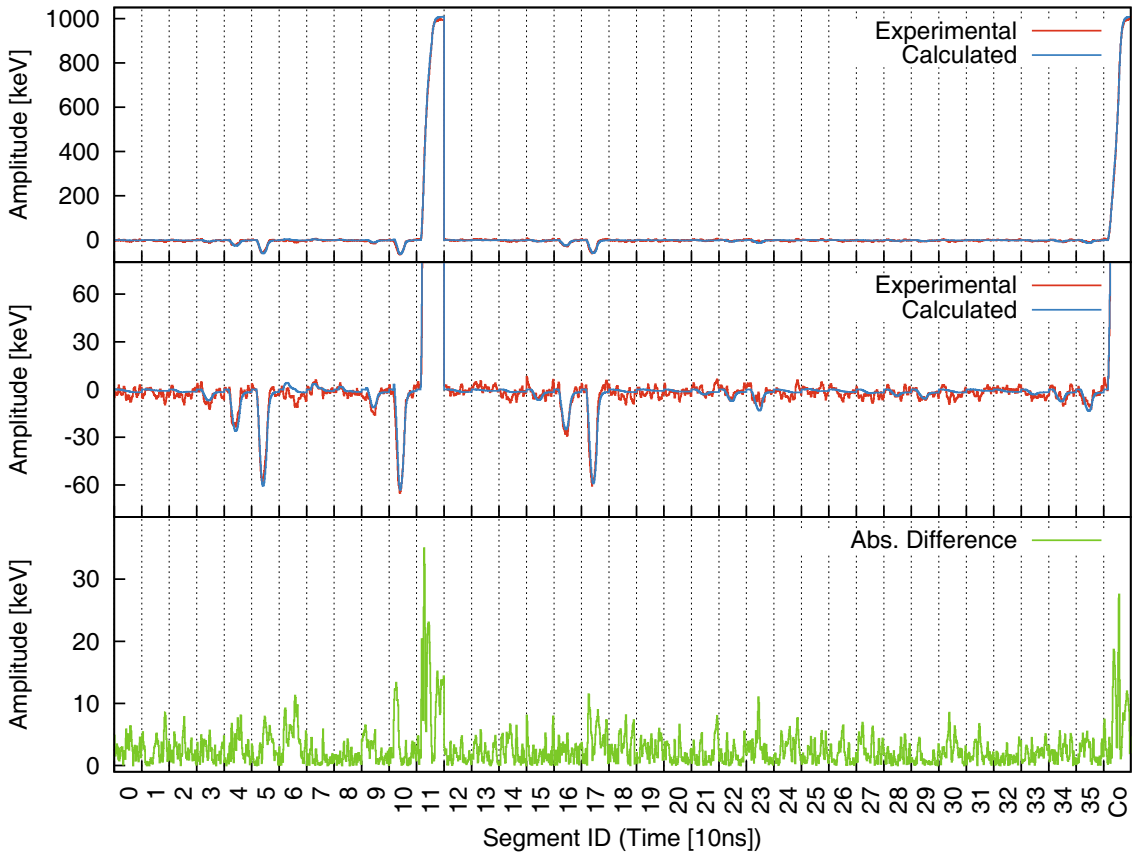

Fig. 5. The best match determined by the grid search algorithm of a random interaction scaled to the right energy compared to experimental data. The horizontal axis is split in 37 sections, each containing a 600 ns trace of the corresponding electrode. Top plot is scaled to full energy deposition. Middle plot is zoomed to emphasize the transient signals. Bottom plot shows the absolute difference between simulation and measurement.

function of the acquisition electronics and the differential crosstalk in the signals of the library.

Up to now the quality of the ADL signal basis is surveyed by several in-beam and source measurements which are sensitive to the position resolution deduced from the signal shapes. The final position resolution depends critically on the quality of the calculated signal bases. To obtain an experimental position resolution different techniques were employed and up to now a final resolution below 5 mm (FWHM) is obtained for a gamma energy above 1 MeV. The technique described in [53] compares a Monte Carlo simulations of the detector response with an experiment performed at the IKP Cologne. In the experiment a ^{48}Ti beam with 100 MeV impinged on a deuterated titanium target. The reaction ^{48}Ti(d, p)^{49}Ti was investigated in inverse kinematics. The γ-rays were measured with the first symmetric AGATA triple. To reconstruct the velocity vector of the scattered nucleus a double-sided silicon strip detector (DSSSD) was used to detect the emitted proton. The performance of the Doppler correction was compared to simulations taking into account the different contributions that cause a broadening of the peak. The final position resolution is of the order of 5 mm at an energy of 1382 keV. This first result was already close to the design performance of 4 mm for AGATA and was clearly improved in the following years.

Another technique employs the imaging capability of AGATA to determine the position resolution of a single AGATA detector [54] and assesses a mean position resolution of 5 mm in an energy range from 300 keV to 1 MeV.

A third approach uses the annihilation of the positron emitted by a ^{22}Na source to extract the position resolution [55]. As the two γ-rays emitted by the annihilation process have opposite directions two AGATA detectors at different locations were used to perform a source measurement. Based on the comparison of Monte Carlo simulations and experimental data different methods were developed to measure mean and individual position resolutions. A position resolution of 3.5 mm was determined for an energy of 511 keV.

A recent publication is based on the Doppler broadening method [20]. The experiment was one of the first commissioning experiments performed with the AGATA setup at LNL. The results show that the FWHM of the interaction position resolution varies nearly linearly as a function of γ-ray energy. For a low γ-ray energy of 250 keV the position resolution is 8.5 mm. However the value is improving at higher energies and reaches 4 mm at 1.5 MeV; this value stays constant up to 4 MeV.

In the near future a detailed comparison between a set of measured position-dependent pulses and the ADL calculations will allow a refined and direct inspection.

5 Summary

New detector arrays for γ-ray spectroscopy are based on segmented HPGe crystals and implement the new method of γ-ray tracking. For this purpose PSA algorithms are employed to obtain the needed position information of the individual γ-ray interactions. PSA algorithms compare experimental and pre-determined data sets. ADL is a computer code used for computation of the vast amount of position-dependent pulses for such libraries. The basic concepts of the signal calculations are presented including experimental details on the measuring of the input parameters like the axis orientation of an AGATA detector. Meaningful approximations are exploited and discussed in this work. The layout of the program package and the different steps needed to calculate a PSA data base are described in detail. The achieved results of the experimentally determined position resolution unambiguously demonstrate that ADL is successfully utilized for spectroscopic investigations which are performed with the AGATA spectrometer.

This research was supported by the German BMBF under Grants 06K-167, 06KY205I and 05P12PKFNE TP4. AGATA was supported by the European funding bodies and the EU Contract RII3-CT-2004-506065.

References

1. J. Eberth, J. Simpson, Prog. Part. Nucl. Phys. **60**, 283 (2008).
2. R. Venturelli, D. Bazzacco, *Adaptive Grid Search as Pulse Shape Analysis Algorithm for γ-Tracking and Results*, LNL Annual Report (2004).
3. Th. Kröll, D. Bazzacco, Nucl. Instrum. Methods A **565**, 691 (2006).
4. A. Olariu *et al.*, Nucl. Sci. IEEE Trans. **53**, 1028 (2006).
5. M. Schlarb, R. Gernhäuser, S. Klupp, R. Krücken, Eur. Phys. J. A **47**, 131 (2011).
6. S. Akkoyun *et al.*, Nucl. Instrum. Methods A **668**, 26 (2012).
7. S. Paschalis *et al.*, Nucl. Instrum. Methods A **709**, 44 (2013).
8. L. Nelson *et al.*, Nucl. Instrum. Methods A **573**, 153 (2006).
9. A.J. Boston *et al.*, Nucl. Instrum. Methods A **604**, 48 (2009).
10. T.M.H. Ha *et al.*, Nucl. Instrum. Methods A **697**, 123 (2013).
11. C. Domingo-Pardo *et al.*, Nucl. Instrum. Methods A **643**, 79 (2011).
12. N. Goel *et al.*, Nucl. Instrum. Methods A **652**, 591 (2011).
13. F.C.L. Crespi *et al.*, Nucl. Instrum. Methods A **593**, 440 (2008).
14. P. Désesquelles, Nucl. Instrum. Methods A **654**, 324 (2011).
15. B. Bruyneel, P. Reiter, G. Pascovici, Nucl. Instrum. Methods A **569**, 774 (2006).
16. A. Wiens, H. Hess, B. Birkenbach, B. Bruyneel, J. Eberth, D. Lersch, G. Pascovici, P. Reiter, H.-G. Thomas, Nucl. Instrum. Methods A **618**, 223 (2010).
17. J. van der Marel, B. Cederwall, Nucl. Instrum. Methods A **437**, 538 (1999).
18. G.J. Schmid *et al.*, Nucl. Instrum. Methods A **430**, 6 (1999).
19. E. Farnea, F. Recchia, D. Bazzacco, Th. Kröll, Zs. Podolyak, B. Quintana, A. Gadea, Nucl. Instrum. Methods A **621**, 331 (2010).
20. P.-A. Söderström *et al.*, Nucl. Instrum. Methods A **638**, 96 (2011).
21. P. Medina *et al.*, `http://www.iphc.cnrs.fr/-MGS-.html`.
22. I. Mateu, P. Medina, J.P. Roques, E. Jourdain, Nucl. Instrum. Methods A **735**, 574 (2014).
23. M. Schlarb, R. Gernhäuser, S. Klupp, R. Krücken, Eur. Phys. J. A **47**, 132 (2011).
24. G. Lutz, *Semiconductor Radiation Detectors*, first edition (Springer, Berlin-Heidelberg-New York, 1999).
25. `http://www.silvaco.fr/`.
26. `http://www.synopsys.com/`.
27. National Institute of Standards and Technology, *Stopping-power and range tables for electrons, protons, and helium ions* (2009).
28. G. Pausch, W. Bohne, D. Hilscher, Nucl. Instrum. Methods A **337**, 573 (1994).
29. Glenn F. Knoll, *Radiation Detection and Measurement*, third edition (John Wiley & Sons, 2000).
30. C. Jacoboni, F. Nava, C. Canali, G. Ottaviani, Phys. Rev. B **24**, 1014 (1981).
31. S. Aydin *et al.*, *Effective size of segmentation lines of an AGATA crystal*, LNL Annual Report (2007).
32. E.L. Hull *et al.*, Nucl. Instrum. Methods A **364**, 488 (1995).
33. P. Mullowney *et al.*, Nucl. Instrum. Methods A **662**, 33 (2012).
34. B. Bruyneel *et al.*, *Determination of the Crystal Orientation of the AGATA Detectors*, LNL Annual Report (2010).
35. L. Mihailescu, W. Gast, R.M. Lieder, H. Brands, H. Jäger, Nucl. Instrum. Methods A **447**, 350 (2000).
36. B. Bruyneel, P. Reiter, G. Pascovici, Nucl. Instrum. Methods A **569**, 764 (2006).
37. W. Blum, W. Riegler, W. Rolandi, *Particle Detection with Drift Chambers*, first edition (Springer, Berlin, Heidelberg, 2008).
38. E. Gatti, G. Padovini, V. Radeka, Nucl. Instrum. Methods **193**, 651 (1982).
39. W. Riegler, Nucl. Instrum. Methods A **535**, 287 (2004).
40. B. Bruyneel, P. Reiter, A. Wiens, J. Eberth, H. Hess, G. Pascovici, N. Warr, D. Weisshaar, Nucl. Instrum. Methods A **599**, 196 (2009).
41. B. Bruyneel *et al.*, Nucl. Instrum. Methods A **608**, 99 (2009).
42. B. Bruyneel, *Pulse shape analysis with the AGATA demonstrator* (Germanium Workshop Berkeley, 2010).
43. B. Bruyneel, PhD thesis, Institut für Kernphysik der Universität zu Köln (2006).
44. `http://www.simion.com`.
45. W.H. Press, B.P. Flannery, S.A. Teukolsky, W.T. Vetterling, *Numerical Recipes in C: The Art of Scientific Computing*, second edition (Cambridge University Press, 1992).
46. `http://www.ikp.uni-koeln.de/agata/`.
47. B. Birkenbach, B. Bruyneel, G. Pascovici, J. Eberth, H. Hess, D. Lersch, P. Reiter, A. Wiens, Nucl. Instrum. Methods A **640**, 176 (2011).

48. B. Bruyneel, B. Birkenbach, P. Reiter, Nucl. Instrum. Methods A **641**, 92 (2011).
49. B. Birkenbach, *Raumladungsverteilungen in hochsegmentierten HPGe-Detektoren*, Diplomarbeit (2009).
50. B. Birkenbach *et al.*, *Determination of the Space Charge Distributions in the AGATA Detectors*, LNL Annual Report 2010 (2010) p. 68.
51. B. Bruyneel *et al.*, Eur. Phys. J. A **49**, 61 (2013).
52. T. Beck, PhD thesis, Fachbereich Physik Johann Wolfgang Göthe-Universität in Frankfurt am Main (2007).
53. F. Recchia *et al.*, Nucl. Instrum. Methods A **604**, 555 (2009).
54. F. Recchia *et al.*, Nucl. Instrum. Methods A **604**, 60 (2009).
55. S. Klupp, Master's thesis, Technical University Munich (2011).